Site-directed Spin-labeling Analysis of Reconstituted *Mscl* in the Closed State

Eduardo Perozo,[1] Anna Kloda,[2] D. Marien Cortes,[1] and Boris Martinac[2]

[1]Department of Molecular Physiology and Biological Physics, University of Virginia, Charlottesville, VA, 22906
[2]Department of Pharmacology, Queen Elisabeth II Medical Center, University of Western Australia, Crawley, WA 6009, Australia

ABSTRACT   The mechanosensitive channel from *Escherichia coli* (*Eco-MscL*) responds to membrane lateral tension by opening a large, water-filled pore that serves as an osmotic safety valve. In an attempt to understand the structural dynamics of *MscL* in the closed state and under physiological conditions, we have performed a systematic site-directed spin labeling study of this channel reconstituted in a membrane bilayer. Structural information was derived from an analysis of probe mobility, residue accessibility to O_2 or NiEdda and overall intersubunit proximity. For the majority of the residues studied, mobility and accessibility data showed a remarkable agreement with the *Mycobacterium tuberculosis* crystal structure, clearly identifying residues facing the large water-filled vestibule at the extracellular face of the molecule, the narrowest point along the permeation pathway (residues 21–26 of *Eco-MscL*), and the lipid-exposed residues in the peripheral transmembrane segments (TM2). Overall, the present dataset demonstrates that the transmembrane regions of the *MscL* crystal structure (obtained in detergent and at low pH) are, in general, an accurate representation of its structure in a membrane bilayer under physiological conditions. However, significant differences between the EPR data and the crystal structure were found toward the COOH-terminal end of TM2.

KEY WORDS: mechanosensitive channel • solvent accessibility • dipolar coupling • EPR • transmembrane segments

INTRODUCTION

MscL, the large conductance mechanosensitive (MS)* channel, provides prokaryotes with a safeguard mechanism in response to hypoosmotic challenges (Levina et al., 1999). *MscL* opens a large aqueous pore in response to cell swelling, allowing the microorganism to quickly release internal osmolytes and, thus, serves as an osmotic "safety valve." Since its molecular identification (Sukharev et al., 1994), *MscL* has been extensively studied by various structural and functional approaches (for review see Hamill and Martinac, 2001). A distinct feature of all prokaryotic MS channels is their ability to gate by mechanical force, transmitted via the membrane lipid bilayer. The activation of *MscL* through a bilayer mechanism (Martinac et al., 1990; Hamill and McBride, 1997) has been amply documented (Martinac et al., 1987, 1990; Sukharev et al., 1993, 1994, 1999; Häse et al., 1995; Blount et al., 1996). Thus, the lipid bilayer is not only the natural matrix of *MscL* as a membrane protein, but it also represents a structural moiety essential for its gating mechanism.

Our understanding of the molecular mechanisms of mechanosensation has been significantly advanced with the recent elucidation of the crystal structure of the MS channel from *Mycobacterium tuberculosis* (*Tb-MscL*) by Chang et al. (1998). The structure shows that *Tb-MscL* is organized as a homopentamer with each subunit formed by two transmembrane segments (TM1 and TM2) and a cytoplasmic helix forming a five-helix bundle (see Fig. 1 C). This structural model has provided an excellent blueprint to rationalize a great deal of functional information that has been accumulated mostly from patch clamp experiments (Sukharev et al., 1997; Batiza et al., 1999; Oakley et al., 1999; Spencer et al., 1999; Rees et al., 2000; Hamill and Martinac, 2001; Martinac, 2001). However, given the critical role that lipid–protein interactions play in *MscL* function, an important question that remains to be answered is the degree to which the X-ray structure of *MscL* determined in detergent micelles (Chang et al., 1998) resembles that in its native environment. As recently demonstrated on a variety of membrane protein systems (Hubbell et al., 2000; Mchaourab and Perozo, 2000), the use of electron paramagnetic resonance (EPR) spectroscopy in combination with cysteine chemistry and site-directed spin labeling provides a powerful method to study the structure and dynamics of ion channels in their native environment. Features of the secondary and tertiary structure of a given protein can be de-

Address correspondence to Dr. Eduardo Perozo, Department of Molecular Physiology and Biological Physics, University of Virginia, Charlottesville, VA, 22906. Fax: (434) 982-1616 E-mail: eperozo@virginia.edu

Abbreviations used in this paper: EPR, electron paramagnetic resonance; MS, mechanosensitive.

duced on the basis of EPR-derived structural parameters at room temperature, under physiological conditions and in the case of membrane proteins, preserving native lipid–protein interactions.

In this study, we describe the structural characterization of TM1 and TM2, the two transmembrane domains of the *Escherichia coli MscL* (*Eco-MscL*) by site-directed spin labeling and EPR spectroscopy on channels reconstituted in artificial liposomes. Our study demonstrates that the secondary structure and membrane topology of *Eco-MscL* largely corresponds to the 3-D crystal structure of *Tb-MscL*. Nevertheless, we also found a few systematic discrepancies between the structures of *Eco-MscL* and *Tb-MscL* toward the COOH-terminal end of TM2, suggesting that the cytoplasmic regions of *MscL* might have a different conformation under physiological conditions. These discrepancies are discussed in conjunction with the differences in the experimental approaches used for the structure determination of the two channel homologues. Preliminary results from this study have been reported in abstract form (Martinac et al., 2000; Perozo et al., 2001).

MATERIALS AND METHODS

Mutagenesis, Expression, and Spin Labeling of MscL

Cysteine mutants were generated for residues 14–43 and 72–107 in *MscL*, covering the predicted length of TM1 and TM2, respectively. Mutagenesis was performed by oligonucleotide mismatch site-directed mutagenesis using the Transformer kit (CLONTECH Laboratories, Inc.) and confirmed by dideoxy DNA sequencing. Mutant channels were expressed and purified as follows: the construct *MscL*-pQE32 containing *MscL* with the RGS-(4× His) epitope at the NH$_2$ terminus was used to transform *E. coli* XL-1 blue cells (Stratagene) using standard chemical methods. After protein expression was induced by addition of 1 mM IPTG, membranes were solubilized in PBS containing dodecyl maltoside (DDM) at room temperature, spun-down at 100,000 *g* for 1 h and purified with a Co^{2+}-based metal-chelate chromatography resin (Talon resin; CLONTECH Laboratories, Inc.). Unless specifically noted, the purified mutant protein was spin labeled overnight with methanethiosulfonate spin label (Toronto Research) at a 10:1 label/channel molar ratio and reconstituted at a 500:1 lipid/channel molar ratio by dilution in PBS (Cuello et al., 1998).

EPR Spectroscopy and Data Analysis

EPR spectroscopy was performed as described previously (Perozo et al., 1998; Cortes et al., 2001). X-band CW EPR spectra were ob-
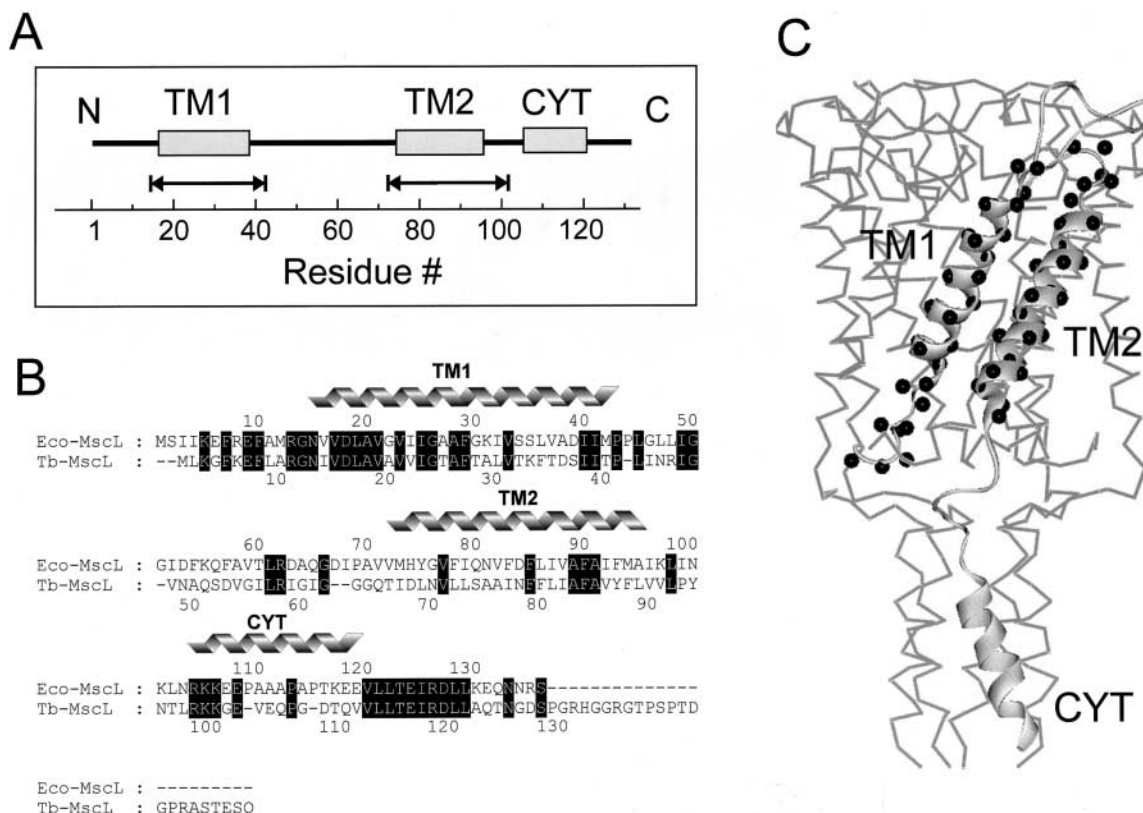

FIGURE 1. (A) Linear representation of the membrane topology of *Eco-MscL*. The helical portions of the *Eco-MscL* monomer (the transmembrane domains TM1 and TM2 and the cytoplasmic helix CYT) are represented by rectangles. The scale corresponds to the amino acid residue numbering. The double-headed arrows designate the amino acid residues replaced by reactive cysteines used for spin labeling. (B) Sequence alignment of *Eco-MscL* and *Tb-MscL*. Identical residues are highlighted (black). The residues corresponding to two transmembrane helical domains (TM1 and TM2) and the cytoplasmic helix (CYT) are marked. (C) Single *MscL* subunit showing amino acid residues subjected to cysteine scanning mutagenesis (black spheres). The single MscL monomer is represented as a part of the channel pentamer according to the 3-D crystal structure of the channel.

tained in a Bruker EMX spectrometer fitted with a loop-gap resonator under the following conditions: 2-mW incident power, 100 kHz modulation frequency, and 1 G modulation amplitude. The accessibility parameter Π (Farahbakhsh et al., 1992) was used in this study to quantify the extent of solvent accessibility in a per residue basis. Π reports on the individual collision frequency of a nitroxide spin label with paramagnetic test compounds, and it is derived from the midpoints of signal saturation at increasing microwave powers according to:

$$I = A\sqrt{P}\left[1 + \frac{(2^{1/\varepsilon}-1)P}{\Delta P_{1/2}(X)}\right]^{-\varepsilon},$$

$$\text{where} \quad \Delta P_{1/2}(X) = P_{1/2}(X) - P_{1/2}(N_2).$$

$P_{1/2}(X)$ is the microwave power at which the peak-to-peak amplitude of the $M_I = 0$ EPR resonant line (the central line), I is half-saturated, P is the microwave power in milliwatts, A is a scaling factor, and ε is a homogeneity parameter. $P_{1/2}(X)$ is measured in the presence of soluble relaxing agents and $P_{1/2}(N_2)$ represents the saturation behavior in the absence of paramagnetic collisions. Power saturation curves were obtained for each spin-labeled mutant after equilibration in N_2 as control, and air (21% O_2), and N_2 in the presence of 200 mM Ni-Edda as relaxing agents. All EPR data were obtained at room temperature.

R E S U L T S

Fig. 1 A shows a schematic representation of an *E. coli* *MscL* subunit, where individual rectangles represent the approximate assignments of the α-helical elements according to the *Tb-MscL* crystal structure. Double arrows depict the extent and location of the cysteine mu-

tant set that forms the basis of this study. There is 36% sequence identity between MS channels from *E. coli* and *M. tuberculosis*. Since they also differ in the total number of residues (136 and 151, respectively), a baseline correspondence between these two sequences is required to support structural comparisons between the present experimental results and the crystal structure. This numerical equivalence is shown in Fig. 1 B, where a ClustalW (Thompson et al., 1994) pairwise sequence alignment between these two sequences is shown.

A total of 66 cysteine mutants comprising both transmembrane segments were used in the present study (30 mutants in TM1, and 36 in TM2). Their equivalent position in the *Tb-MscL* structure is depicted by black spheres on a ribbon diagram of the monomer (Fig. 1 C). Each mutant was expressed, purified, labeled, and reconstituted into asolectin liposomes before their analysis by EPR spectroscopy. In the vast majority of cases, expression levels of the cysteine mutants were essentially identical to that of the wild-type channel. At some positions, cysteine mutagenesis produced a moderate (residues 22 and 26 in TM1; and residues 72, 92, and 95 in TM2) to severe (residues 43, 76, and 78) reduction in expression levels. However, in all cases, *E. coli* growth rates remained unchanged, suggesting that none of the cysteine mutants produced significant gain-of-function effects in *MscL*. This result confirms
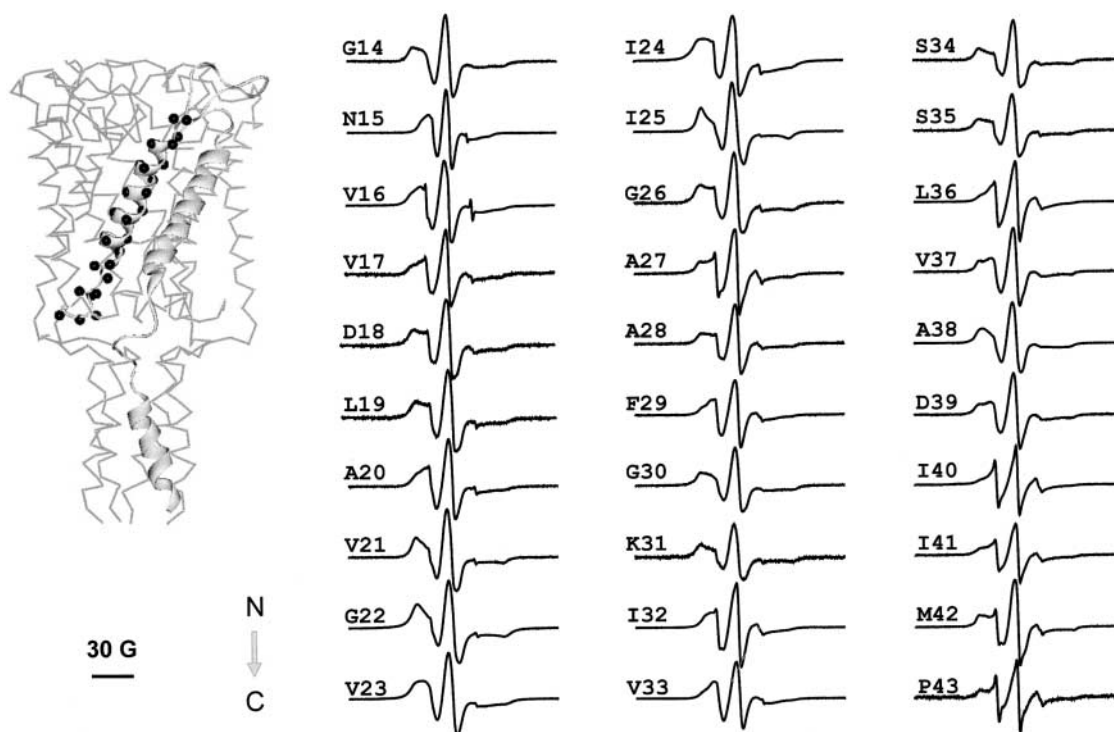

FIGURE 2. X-band EPR spectra of spin-labeled mutants from the first transmembrane domain TM1 of *Eco-MscL* reconstituted into asolectin liposomes. All spectra were obtained using loop-gap resonator with the microwave power of 2 mW and field modulation of 3 G. Spectra are arranged sequentially from the NH₂- to the COOH terminus of the *MscL* monomer in the direction of the arrow. The *MscL* monomer with mutated residues (black spheres) is presented within the 3-D crystal structure of the channel (left). The scale bar corresponds to 30 G.

recent functional analysis on *MscL* cysteine mutants (Yoshimura et al., 2001), and suggests that under the condition of zero transbilayer pressures used in this study, *MscL* is most likely in the closed configuration for all tested mutants.

The structural and membrane topological study of both *MscL* TM segments was based on an analysis of spectral line shape properties on a per-residue basis. Motional information was obtained from an empiric analysis of the EPR line shape reflecting the degree of motional restriction of the nitroxide spin label, and quantified using the inverse of the width of the central resonance line ΔH_0^{-1} (Mchaourab et al., 1996; Columbus et al., 2001). Solvent accessibilities are estimated from power saturation experiments performed in the presence of either atmospheric oxygen or a water-soluble, neutral Ni^{2+} chelate complex (NiEdda). Collision with either probe results in an effective increase in the T1 relaxation rate, which is detected by changes in the extent of signal saturation measured at increasing microwave intensities (Subczynski and Hyde, 1981). Whereas high accessibility to molecular oxygen O_2 (ΠO_2) is indicative of a residue exposed to membrane lipids; residues exposed to the aqueous environment display high NiEdda (Π_{NiEdda}) accessibilities.

Additionally, an estimation of intersubunit proximities was performed from a qualitative analysis of electron spin–spin interactions. Through-space spin–spin coupling is estimated from the degree of spectral broadening present in samples with two or more paramagnetic centers, compared with that of each individual spectra. It has a distance dependence proportional to R^{-3} with a practical range between ~8 and ~25 Å. Unfortunately, in a system with multiple potential labeling sites as *MscL*, only proximity estimates can be obtained. These types of data form the core of most EPR-based structural analysis, from which features related to a protein secondary and/or tertiary structure can be deduced (for reviews see Hubbell et al., 2000; Mchaourab and Perozo, 2000).

TM1 Residue Environmental Parameters

Fig. 2 shows the complete spectral dataset for TM1. An overview of the different types of observed line-shapes reveals a six-residue segment (positions 21–27) in which the spectra appear considerably broadened. Evaluation of the mobility parameter ΔH_0^{-1} from the EPR spectra obtained for the TM1 segment confirms this impression (Fig. 3, top). Additionally, it reveals a strong periodicity in the mobility of the spin label from neighboring amino acid residues, a behavior consistent with the observed α-helical structure of the first transmembrane domain in the crystal structure (L19–A38 in *Tb-MscL*). This periodicity includes even the highly immobilized stretch of residues 21–27 (although with a
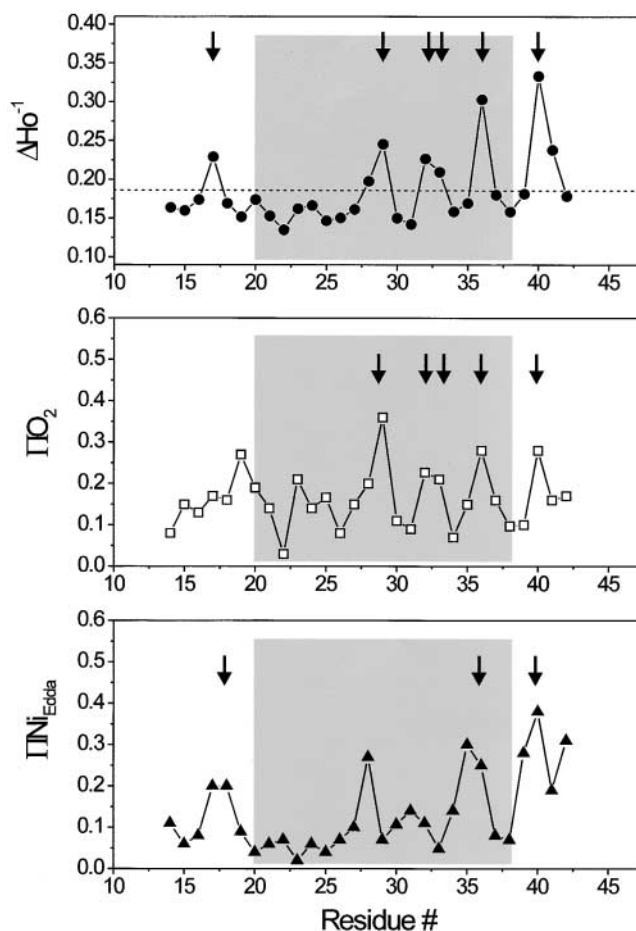

FIGURE 3. Residue-specific environmental parameter profiles obtained for the first transmembrane domain TM1: mobility parameter ΔH_0^{-1} (top, closed circles), oxygen accessibility parameter ΠO_2 (middle, open squares), and NiEdda accessibility parameter $\Pi NiEdda$ (bottom, closed circles). The average mobility for the entire segment is shown in the top panel as a dotted line. Arrows point to those residues with in-phase accessibility and/or probe mobility peaks.

reduced dynamic range). In spite of the closed packing arrangement for the TM1 segment seen in the *Tb-MscL* crystal structure, starting at position 29, there is a gradual increase in the mobility parameter through I40. We have interpreted this observation to suggest that the spin labels at these locations are able to resolve the subtle changes in motional dynamics derived from the gradual increase in the diameter of the outer vestibule of the channel. A similar mobility gradient is observed in TM2 and correlates well with the idea that the most immobilized regions of the channel are toward the cytoplasmic ends (where the gate is proposed to be).

The periodic structure of the TM1 segment is also reflected in the O_2 accessibility profile, where the data shows very low O_2 collision frequencies for every third or fourth residue along the entire TM1 segment (Fig. 3, middle). Interestingly, significant rates of O_2 collision are observed even within the highly immobilized region
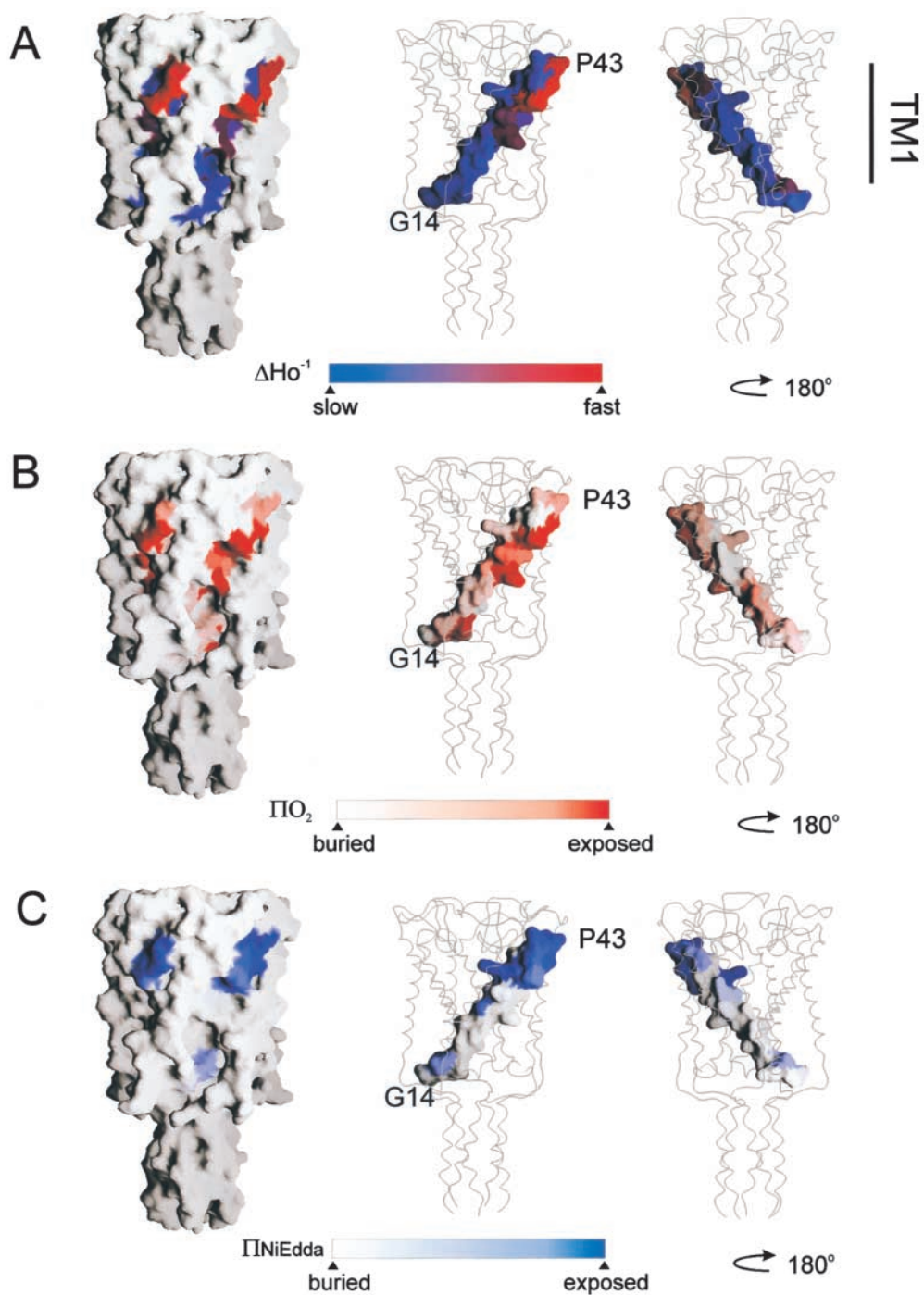
FIGURE 4. Residue environmental parameter profiles for TM1 mapped on equivalent positions of the *Tb-MscL* crystal structure. (A) Mobility parameter ΔH_o^{-1}; (B) oxygen accessibility parameter ΠO_2; and (C) NiEdda accessibility parameter ΠNiEdda. Two views of the mapped parameters of TM1 are shown rotated 180°. In each case, surface accessible representation of whole *MscL* and of TM1 only was done using the program Grasp (Nicholls et al., 1991).

comprised by residues 21–27. As seen in other membrane proteins (for reviews see Perozo et al., 1998; Cortes et al., 2001), O_2 appears to penetrate with some ease into motionally restricted spaces, partially reducing contrast in the determination of angular frequencies.

The NiEdda accessibility profile correlates well with the mobility data, revealing a region of eight residues (positions 19–26), for which accessibility to NiEdda is severely restricted (Fig. 3, bottom). This result is in very good agreement with the *Tb-MscL* crystal structure. Res-

idues in this region of the channel form a hydrophobic constriction zone forming the narrowest point along the permeation path with a diameter of $\sim$2 Å. This area is likely to form a significant barrier to the passage of ions and other solutes, thus, contributing to form the "gate" that physically closes *MscL* channels.

A remarkable observation, also derived from the NiEdda accessibility profile, is the presence of residues along TM1 with significant (even high) NiEdda collision frequencies (positions 28, 31, 35, and 36). These
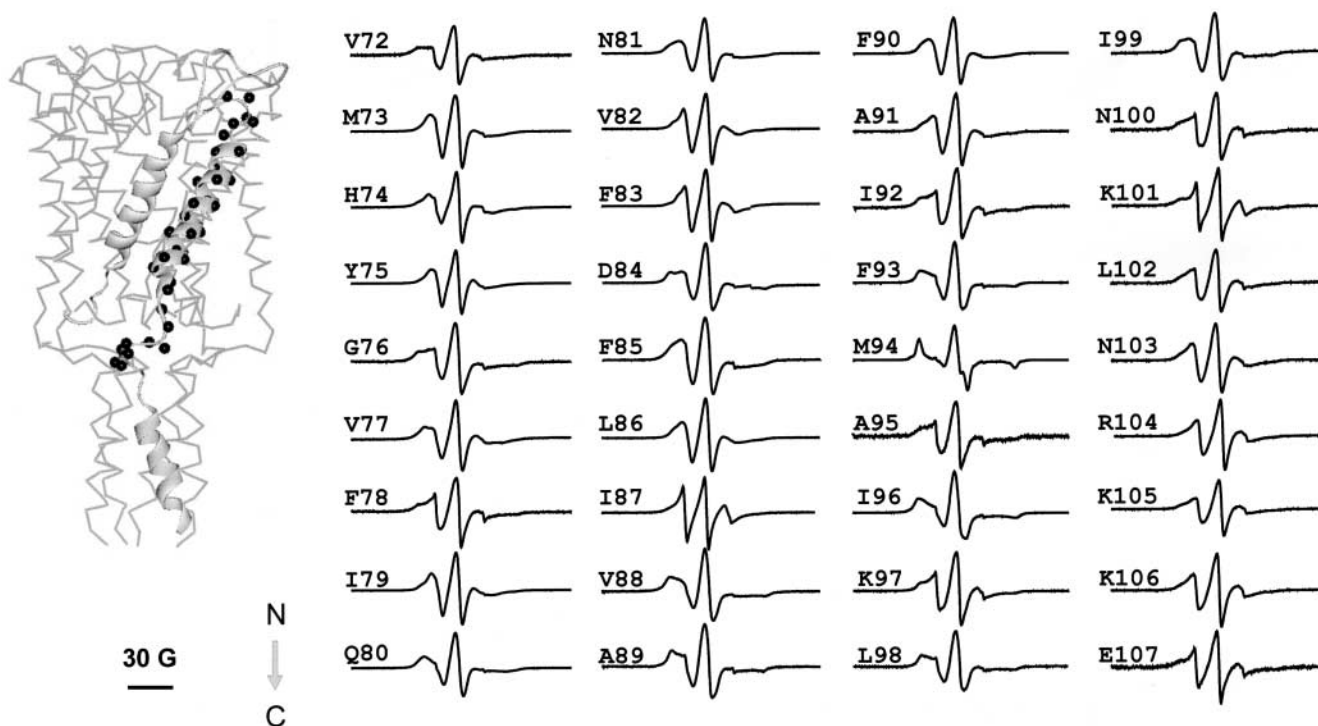
FIGURE 5. X-band EPR spectra of spin-labeled mutants from the second transmembrane domain TM2 of *Eco-MscL* reconstituted into asolectin liposomes. The spectra were obtained using a loop-gap resonator with the microwave power of 2 mW and field modulation of 3 G. The spectra are arranged sequentially from the NH_2 terminus to the COOH terminus of the *MscL* monomer as pointed by the arrow. The *MscL* subunit with mutated residues (black spheres) is superimposed onto the 3-D *MscL* structure (left). The scale bar corresponds to 30 G.

residues are located well within the membrane-embedded portions of TM1, and are a clear manifestation of the large water-filled extracellular vestibule observed in the *Tb-MscL* crystal structure. The fact that the ΠO_2 (a probe of hydrophobicity) and NiEdda (a probe of hydrophilicity) profiles are essentially 180° out of phase confirms that the TM1 segment simultaneously surrounds an aqueous pore while exposed to the membrane phospholipids. This is clear only for the COOH-terminal half of the helix, as increasing protein–protein contacts among TM1 segments and between TM1 and TM2 segments significantly restrict solvent accessibility in the remainder of the helix.

The correlation between the EPR-derived environmental parameters and their location within the crystal structure is shown in Fig. 4, where the unprocessed data for ΔH_0^{-1}, ΠO_2, and Π_{NiEdda} are mapped onto their equivalent positions in *Tb-MscL*. In each case, the property mapped is shown in the context of a solvent-accessible surface representation (1.4-Å probe size) of the full-length channel, and as solvent-accessible surface of TM1 only (in two orientations, rotated 180°).

TM2 Residue Environmental Parameters

Fig. 5 shows a family of EPR spectra from residues V72 to E107, encompassing the length of the TM2 segment

and a portion of the intracellular loop. From these spectral line-shapes, it appears that this segment, as a whole, is slightly less motionally restricted than TM1. This is to be expected from a region of the channel that is predicted to contact the more motionally dynamic environment of the membrane lipids. As is typically the case for protein regions that contact only two different environments, the ΔHo^{-1} profile (Fig. 6, top) shows a remarkably periodic behavior. When analyzed by Fourier methods, the power spectrum for this mobility profile (residues 72–96) reveals a single peak centered at 102° and with a periodicity index of 3.67 (data not shown), in broad agreement with the structure of TM2 derived from the X-ray data (Chang et al., 1998). Unexpectedly, the last turn of the helix, at the COOH-terminal end of TM2, appears to deviate from the preceding periodic behavior, particularly at positions 93 and 94, where line-shapes appear far more motionally restricted than expected on the basis of the crystal structure (see discussion). This particular periodic pattern is mirrored, almost perfectly, by the oxygen accessibility parameter ΠO_2 (Fig. 6, middle), confirming not only that TM2 is at the periphery of the channel, but also that the majority of its residues are directly in contact with the membrane lipid.

Equivalent to what is seen at the COOH-terminal half of TM1, high NiEdda collision frequencies are ob-
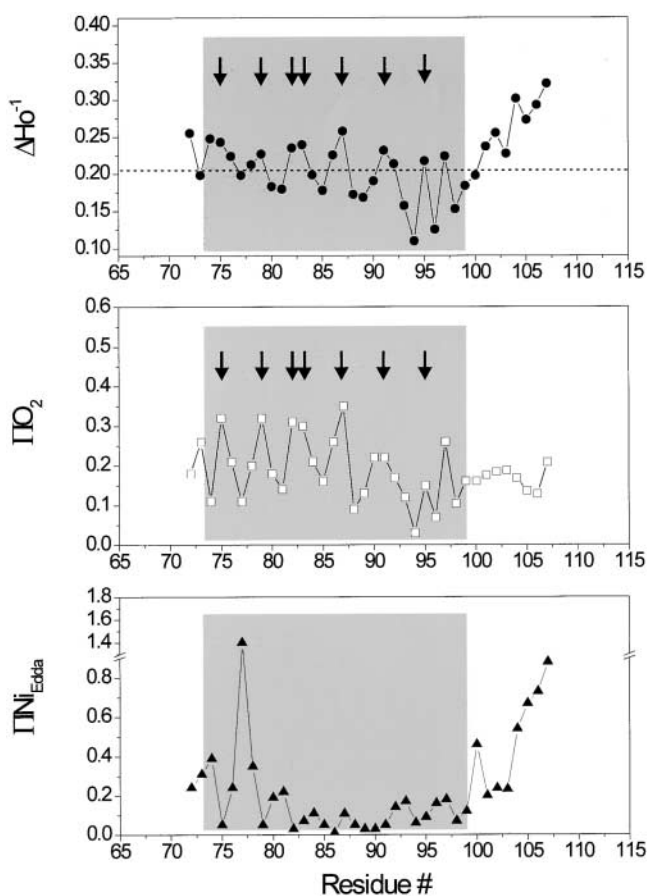
FIGURE 6. Residue-specific environmental parameter profiles obtained for the second transmembrane domain TM2: mobility parameter ΔH_o^{-1} (top, closed circles); oxygen accessibility parameter ΠO_2 (middle, open squares); and NiEdda accessibility parameter $\Pi NiEdda$ (bottom, closed circles). The dotted line in the top panel represents the average ΔH_o^{-1} value for the entire segment. Arrows point to those residues with in-phase accessibility and/or probe mobility peaks.

served at the NH$_2$-terminal end of TM2, a region expected to be fully embedded in a hydrophobic environment (Fig. 6, bottom panel). In both cases, this pattern of accessibility to the aqueous medium occurs 180° out of phase with the ΠO_2 profile, and originates from the presence of the large water-filled vestibule in the extracellular region of the channel. NiEdda accessibility decreases dramatically toward the COOH-terminal end of TM2, reflecting the local environment of residues that contact either lipid or neighboring TM1 segments. A sharp increase in NiEdda accessibility for residue 100 signals the likely point where this TM segment exits the membrane interface. Yet, position 96 corresponds to the last truly helical residue as described in the *Tb-MscL* structure. This segment is immediately followed by a region of progressively larger motional freedom, very high NiEdda accessibility and relatively flat O$_2$ accessibility, all diagnostic properties of aqueous loop-like

structures. These points are well illustrated in Fig. 7, where EPR-derived residue environmental data are mapped onto the *Tb-MscL* crystal structure (parameters of the probe size and color mapping are identical to those of Fig. 4). In the case of the ΔH_0^{-1} and ΠO_2 maps, the dotted squares points to residues in TM2 where experimental values were found to be much lower than expected (positions 93 and 94).

As shown by Altenbach et al. (1994), Φ, the natural log of the ratio between the $\Delta P_{1/2}$ obtained in the presence of O$_2$ and in the presence of NiEdda, is directly proportional to the immersion distance from the membrane–water interface. Thus, with proper calibrations, this value can be used to estimate immersion depths for a series of solvent-exposed residues in a given transmembrane segment. Calculated only for TM2 residues with high collision rates (Fig. 8), these depth estimates strongly suggest that *MscL* can be positioned within the context of a membrane bilayer with residues 86–87 at or very close to the center of the bilayer.

Intersubunit Spin–Spin Interactions

In an oligomer with radial symmetry and a single spin label per subunit, only those residues in close proximity to the symmetry axis are expected to show strong spin–spin coupling. Because of the fivefold symmetry in *MscL*, the spectral broadening from fully labeled channels originates not only from the spin–spin interactions between a given subunit and its immediate neighbors, but also from diagonally related subunits at two different positions. Therefore, spectral broadening derived from spin coupling cannot be easily used in the determination of actual intersubunit distances. In this situation, rather than estimate individual distances, one can establish the unique pattern of proximities present in a given multisubunit system. A gross indication of intersubunit proximities can be obtained from the Ω parameter (Perozo et al., 1998), which is extracted from the extent of the spectral broadening of a fully labeled sample relative to one with no spin–spin interactions (typically underlabeled).

Maximally labeled and underlabeled spectra from selected residues along TM1 (Fig. 9 A) illustrate the point. When labeled at a 10:1 molar ratio of *MscL* monomer to spin label, the vast majority of the labeled channels are predicted to have a single nitroxide group and, hence, represents the unbroadened spectra (Fig. 9 A, red traces). Reversing the labeling ratio (1:10 molar ratio, monomer to spin label) maximizes the likelihood that all available cysteines will be modified with a spin label, thus, assuring broadened spectra (Fig. 9 A, black traces). Application of this type of analysis generates an intersubunit interaction profile (Fig. 9) pointing to residues likely to be located near the symmetry axis of *MscL* (its permeation path). Results from the
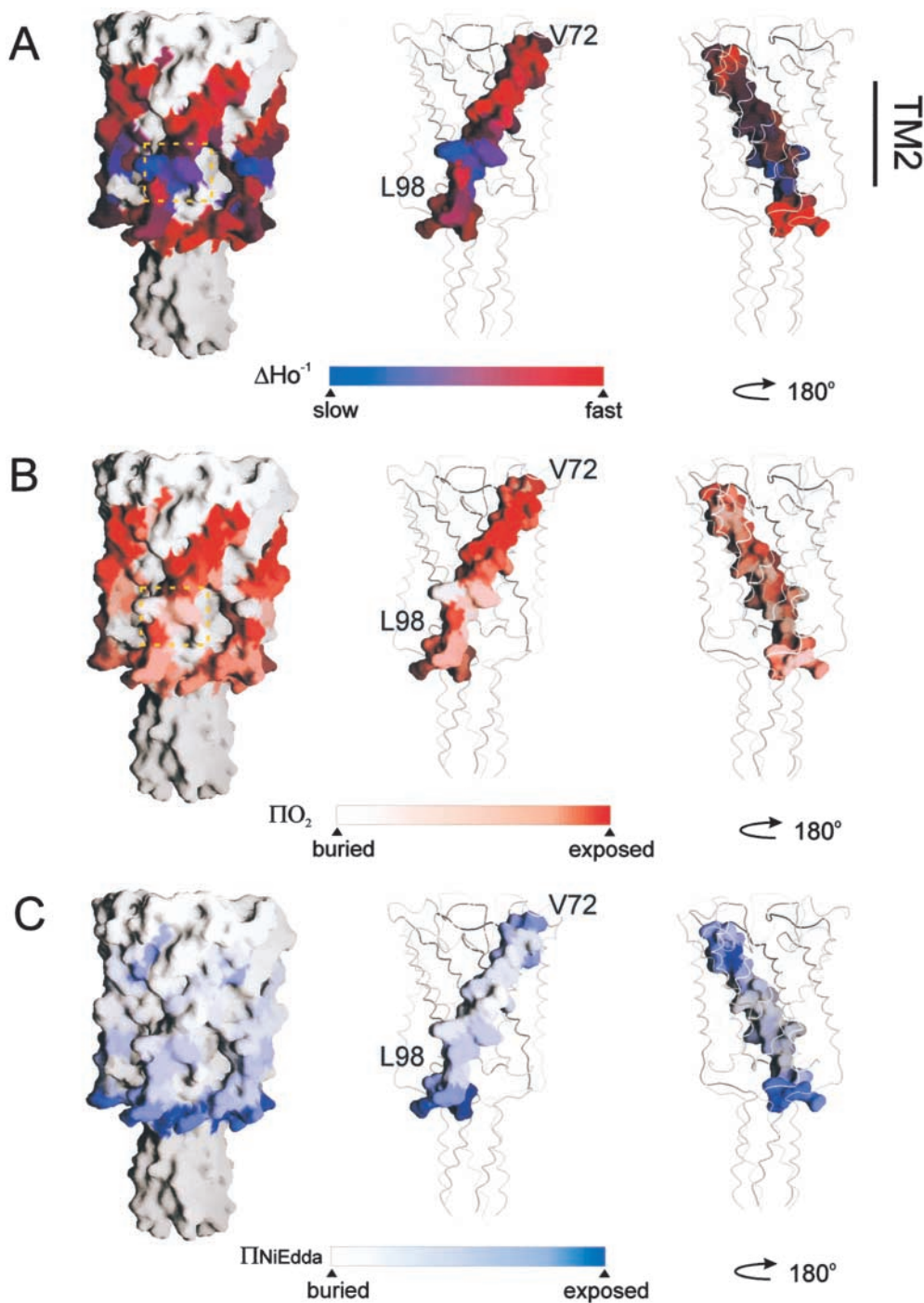
FIGURE 7. Residue environmental parameter profiles for TM2 mapped on equivalent positions of the *Tb-MscL* crystal structure. (A) Mobility parameter ΔH_o^{-1}; (B) oxygen accessibility parameter ΠO_2; and (C) NiEdda accessibility parameter ΠNiEdda. Two views of the mapped parameters of TM1 are shown rotated 180°. In A and B, the dotted squares indicate residues with lower experimental environmental parameters than those expected from the crystal structure. Figure parameters are identical to those in Fig. 4.

TM1 segment (Fig. 9, top) reveal a prominent cluster of interacting residues at positions 20–26, in remarkable agreement with the mobility and NiEdda accessibility data (Fig. 3, top and bottom), suggesting a hydrophobic constriction among these residues. Significant levels of spectral broadening were also observed, with an impressive α-periodicity, at both sides of the major cluster. Surprisingly, we were able to detect small, but significant, levels of spin–spin interactions among residues in the COOH-terminal half of TM2, suggesting

that this side of the TM2 helix is likely to face the symmetry axis (Fig. 9, bottom). The spatial distribution of these interacting residues within *MscL* is illustrated in Fig. 9 C, where Ω values obtained for residues in both TM segments are mapped into the *Tb-MscL* structure, either in ribbon representation or in a cross-section of an accessible surface representation. It is worth noting that the strongest Ω values from the 20 to 26 cluster forms an unmistakable ring around the narrowest section of the *MscL* permeation path, strongly suggesting
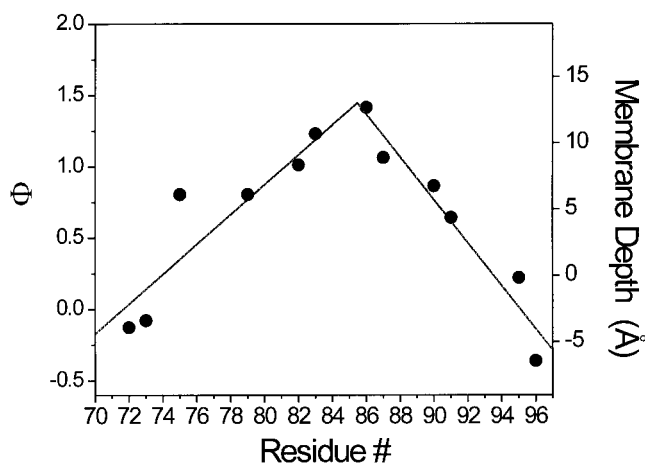
FIGURE 8. Immersion depth for exposed residues in TM2. Individual data points were calculated from a calibration curve of spin-labeled phospholipids following the equation $\Phi = \ln(\Pi(O_2)/\Pi(NiEdda)) = \alpha D + C$, where $\Pi(O_2)$ and $\Pi(NiEdda)$ are accessibility parameters for O_2 and NiEdda, respectively, α is the slope, D is the immersion depth, and C is the intercept. Positive distances indicate immersion toward the center of the bilayers, relative to the membrane interface. Negative values have a very large uncertainty associated and are shown for reference purposes.

that this section of the channel physically contributes to restrict solute permeation in the closed state.

DISCUSSION

The main goal of the present study was to provide an initial assessment of the structural dynamic properties of *MscL* channels in the closed state. This was done using spin labels to report on the local residue environmental properties along the two transmembrane segments of *Eco-MscL* reconstituted in lipid vesicles. This information was then compared with the current crystallographic model from *Tb-MscL* to establish the relevance of this model to the configuration of the closed channel under physiological conditions.

An examination of Figs. 4 and 7 suggests that our solvent accessibility determinations, when mapped onto the *Tb-MscL* crystal structure, conform quite well to expected patterns of surface distribution. The only apparent exception being the unusually low accessibility values for residues located at the COOH-terminal end of TM2. A quantitative comparison between these two structural views of *MscL* can be obtained by contrasting the static solvent-exposed areas of individual residues (calculated from the crystal structure), with their EPR experimentally determined values (Fig. 10). Solvent-exposed areas were obtained using an algorithm based on the Gauss-Bonnet theorem (GETAREA; Fraczkiewicz and Braun, 1998), using a series of probe radii, from 1.4 Å to the algorithm's limit of 4.5 Å. These numbers were compared with NiEdda accessibilities in the case of

TM1 (with a 4.5-Å probe; Fig. 10 A) and to O_2 accessibilities for the peripherally located TM2 (using a 2-Å probe; Fig. 10 B). In TM1, there is a very good overall agreement between the EPR data (Fig. 10, A and B, open circles) and the calculated accessibilities (Fig. 10, A and B, gray squares), although it is clear from this comparison that methods based on hard-sphere area determinations tend to underestimate the actual residue accessibility of a given probe under dynamic conditions. Identical results were obtained using an alternative solvent accessibility algorithm (DSSP; Kabsch and Sander, 1983).

A similar analysis performed on TM2 produced excellent agreement between experimental and calculated accessibilities for a large section of the helix (residues 72–100), but also revealed a major discrepancy for residues 91–95 (Fig. 10 B; see also Fig. 4). These results can be explained as either a phase change from the preceding α-periodicity in residues 72–90, the consequence of a tightly bound molecule within the membrane-embedded regions of the channel, or as the result of protein–protein interaction with other elements of the channel. Furthermore, a review of the spectral line-shapes of residues F93, M94, and A95 also suggest an incompatibility between their dynamic behavior, predicted from the crystal structure, and the present EPR data (Fig. 10 C). Perhaps the most extreme example is residue M94, where the crystal structure predicts a fully extended side chain, away from the symmetry axis and toward the membrane lipids, yet the EPR spectrum is almost as immobilized as in the rigid limit.

What might be the origin of this discrepancy? The presence of additional electron density surrounding *Tb-MscL* crystals (Chang, G., R.H. Spencer, and D.C. Rees, personal communication) has been suggested to correspond to immobilized lipids. If the binding interaction of these molecules is extensive enough, and its dynamics slow in the EPR time scale, these lipid molecules could partially explain the discrepancies in nitroxide mobilities for residues in the last turn of the TM2 helix. However, it would be more difficult to explain the observed disagreement in the accessibility values. The obvious alternative explanation requires the existence of protein–protein interactions not observed in the present *MscL* crystal structure. Clearly, without further EPR analysis of additional regions in *MscL* it is difficult to pinpoint the actual cause of these differences. However, an obvious possibility is that the cytoplasmic regions of the channel might physically interact with TM2 near the membrane interface. One candidate could be the NH_2-terminal end, a segment of ~12 residues that is not resolved from the present crystallographic data. Alternatively, the COOH terminus might not assemble into the cytoplasmic five-helix bundle observed in the crystal structure and, instead, it could fold toward the membrane interface, establishing specific tertiary contacts with TM2. It is
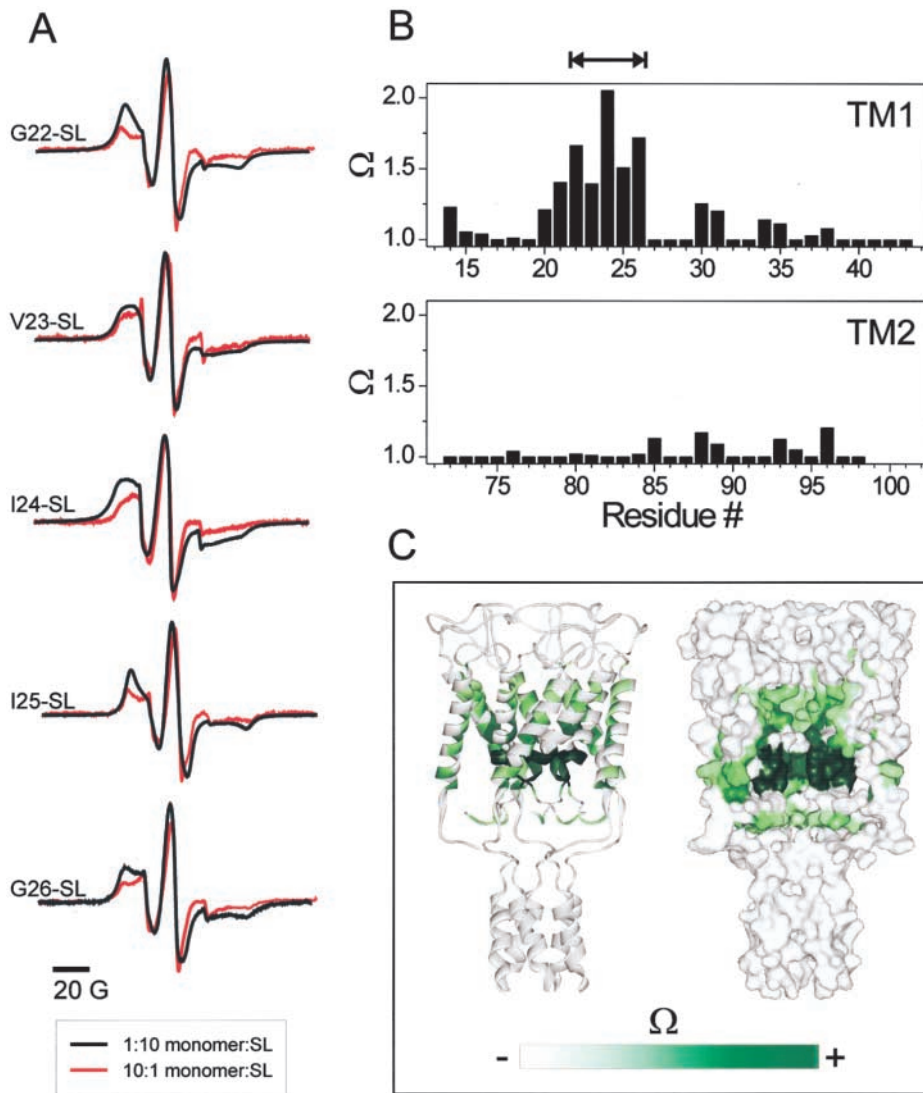
FIGURE 9. Intersubunit electron spin–spin coupling in *MscL*. (A) selected residues along TM1 showing different degrees of spectral broadening due to spin–spin coupling. Traces in black were obtained from fully labeled channels (mole/mole labeling ratio, 10:1 spin label/subunit). Traces in red were obtained from underlabeled channels and represent unbroadened spectra (mole/mole labeling ratio, 1:10 spin label/subunit). (B) Pattern of intersubunit proximities derived from the Ω parameter (top, TM1; bottom, TM2). The double arrow line points to a stretch of hydrophobic residues with restricted mobility. (C) Data in B as mapped onto the equivalent positions in the *Tb-MscL* structure.

important to note that the *Tb-MscL* crystallization experiments were performed at a very low pH (between 3.6 and 3.8; Chang et al., 1998).

Not counting the contributions of the NH_2 terminus, the cytoplasmic-exposed regions of *MscL* are highly charged (9 basic and 7 acidic residues in *Eco-MscL*), and some of these residues form part of a highly conserved charged cluster of residues present not only in all the *MscL* homologues identified to date, but also in all members of the recently identified family of prokaryotic MS channels (Kloda and Martinac, 2001). The physiological function of this charge cluster is yet to be established. It is possible that under the low pH conditions promoting crystal formation, the E104 glutamic acid residue of *Tb-MscL* (E109 in *Eco-MscL*) is protonated, thus, stabilizing the Tb-MscL cytoplasmic helical bundle. At pH values closer to neutral one might expect these and other negative charges to contribute to the electrostatic destabilization of this bundle. Although preliminary evidence

from molecular dynamics simulations tends to support this interpretation (Elmore et al., 2001), at the moment there is no direct structural evidence addressing this point. Interestingly, intracellular pH is known to significantly modulate the pressure sensitivity of MS channels in general (Hamill and Martinac, 2001), such that in patch-clamp experiments performed at a low pH, MscL becomes less sensitive to membrane tension compared with its sensitivity to pressure at neutral pH (unpublished data). Thus, it is possible that the formation of the cytoplasmic helical bundle under low pH conditions will tend to stabilize the closed state.

It is important to define which regions of *MscL* physically contribute to form the gate that so effectively blocks solute flow at rest, but is able to undergo such massive conformational change that leads to an open conduction pore of 30–40 Å in diameter (Cruickshank et al., 1997; Ajouz et al., 1998). By applying the VIOIDOO/FLOOD program (Kleywegt and Jones, 1994) to
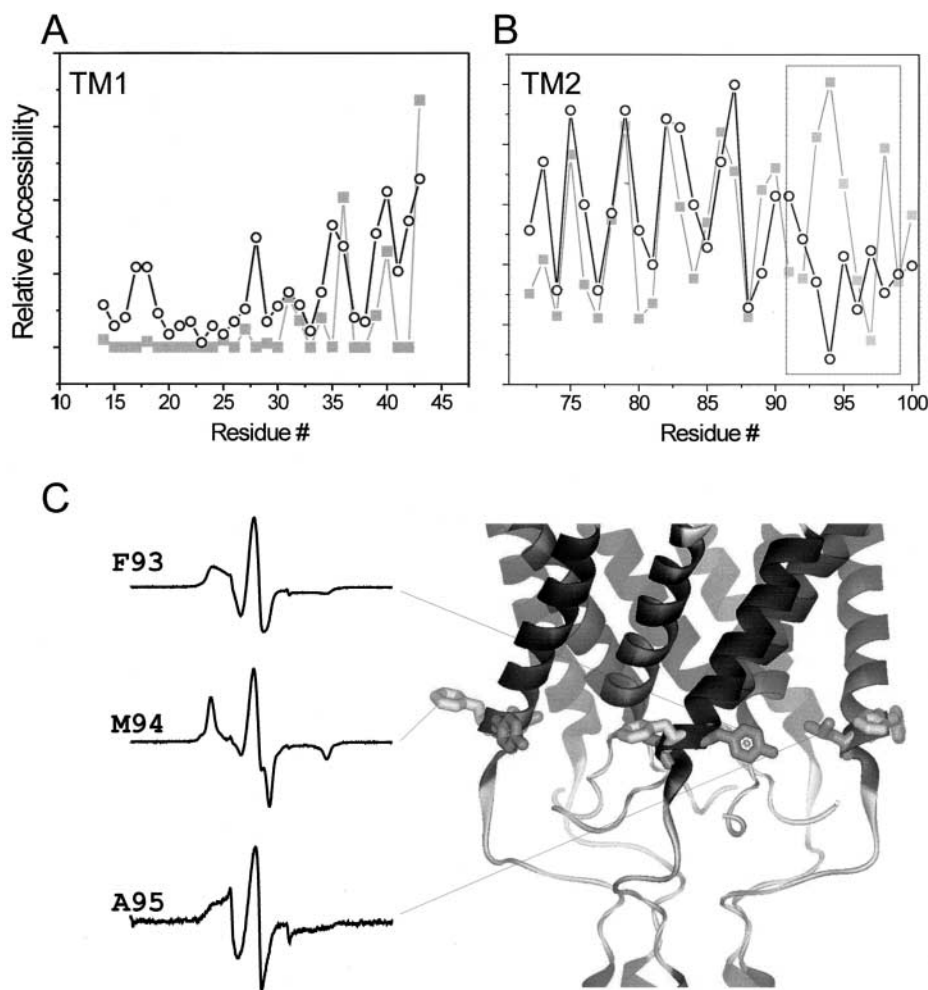
FIGURE 10. Comparison between experimental and calculated solvent accessibilities. (A) Experimentally determined Ni-Edda accessibility along TM1 (open circle) compared with the per-residue accessibility calculated using the program GETAREA (Fraczkiewicz and Braun, 1998) using a 4.5-Å probe (closed square). (B) Experimentally determined O_2 accessibility along TM2 (open circle) compared with the calculated accessibility using a 2-Å probe (closed square). The dotted rectangle points to a region of clear discrepancy between the EPR data and the crystal structure at the equivalent position (C) EPR spectra and location of the positions highlighted in B accompanied by their respective spectra.

the *Tb-MscL* crystal structure, it was estimated that in the closed conformation MscL could be filled with water molecules to a point 24 Å below the periplasmic surface of the channel pentamer (Oakley et al., 1999). Similarly, the second cavity at the cytoplasmic surface of the channel was found to be accessible to water. Thus, most of the inside of the closed *MscL* could be filled with water with the exception of an 8-Å segment that corresponds to the hydrophobic constriction formed by TM1 residues. This hydrophobic constriction correlates very well with a stretch of amino acids (residues A20–G26) that show characteristically low mobility (Fig. 3, top), low NiEdda accessibility (Fig. 3, bottom), and significant spin–spin coupling (Fig. 9 B). This result is also in good agreement with the findings of several functional mutagenesis studies on *Eco-MscL*, which indicated that the channel gate is likely to be formed by the hydrophobic constriction that includes residues V21 and G22 (Moe et al., 1998; Yoshimura et al., 1999). Thus, the region of the channel where the actual barrier to conduction occurs is quite thin compared with the ∼35-Å thickness of the membrane bilayer.

A recent model for the gating mechanism of *MscL* in-

troduced the notion that the NH_2 terminus might form a second external gate in addition to the hydrophobic gate formed by the TM1 segments (Sukharev et al., 2001). According to this proposal, the NH_2 terminus has a helical structure and is mobile, which should facilitate its interaction with the TM1 and TM2 segments with which it forms part of the channel's lining in the open conformation. Although not dealing directly with this region of *MscL*, our present data does not contradict this model. Indeed, the spin–spin interaction parameter Ω calculated for the residues G14 and N15 (Fig. 9 B), which according to the model form a part of the S1-M1 linker, indicates some degree of spin–spin coupling for these residues, as expected for regions of the channel adjacent to the permeation path. The mobility and structural role of the NH_2 termini in the *MscL* pentamer, however, requires additional analysis for which the present approach appears ideally suited.

Having established a spectroscopic "native dataset" for *MscL* in the closed configuration, we are in position to undertake an analysis of its gating mechanism from a structural standpoint. Some of the key issues that remain to be established include not only the types and

directions of the molecular rearrangements that underlie channel opening, but also the fundamental physical mechanisms that allow the transduction of bilayer deformations into protein movement. It is perhaps the answer to this last question what could make possible a spectroscopic analysis of *MscL* gating, since a key challenge in such a project is in fact the ability to stabilize the open state under zero transbilayer tensions. It will be critical to understand the extent to which the internal bilayer forces (hydrophobic mismatch, membrane intrinsic curvature) contribute to trigger *MscL* gating.

In conclusion, we have characterized the structural dynamic properties of the transmembrane elements of *MscL* using site-directed spin labeling and EPR spectroscopy. Our results establish the overall structural validity of the recent crystal structure as a model for the membrane-embedded regions of *MscL* in their natural environment. Nonetheless, substantial inconsistencies in residue environmental parameters toward the COOH-terminal end of the TM2 helix seem to suggest that this agreement might not hold toward the soluble, cytoplasmic-facing regions of the channel under physiological conditions. Consequently, our findings emphasize the advantage of alternative (even if lower resolution) methods in the determination of higher order structures of membrane proteins under conditions that closely reflect the protein native membrane environments. Furthermore, this study sets the stage for a structural analysis of the gating mechanism in this class of MS channels.

REFERENCES

Ajouz, B., C. Berrier, A. Garrigues, M. Besnard, and A. Ghazi. 1998. Release of thioredoxin via the mechanosensitive channel MscL during osmotic downshock of Escherichia coli cells. *J. Biol. Chem.* 273:26670–26674.

Altenbach, C., D.A. Greenhalgh, H.G. Khorana, and W.L. Hubbell. 1994. A collision gradient method to determine the immersion depth of nitroxides in lipid bilayers: application to spin-labeled mutants of bacteriorhodopsin. *Proc. Natl. Acad. Sci. USA.* 91:1667–1671.

Batiza, A.F., I. Rayment, and C. Kung. 1999. Channel gate: tension, leak and disclosure. *Struct. Fold. Design* 7:R99–R103.

Blount, P., S.I. Sukharev, P.C. Moe, M.J. Schroeder, H.R. Guy, and C. Kung. 1996. Membrane topology and multimeric structure of a mechanosensitive channel protein of *Escherichia coli. EMBO J.* 15:4798–4805.

Chang, G., R.H. Spencer, A.T. Lee, M.T. Barclay, and D.C. Rees. 1998. Structure of the MscL homolog from *Mycobacterium tuberculo-*

sis: a gated mechanosensitive ion channel. *Science.* 282:2220–2226.

Columbus, L., T. Kálai, J. Jekö, K. Hideg, and W.L. Hubbell. 2001. Molecular motion of spin labeled side chains in α-helices: analysis by variation of side chain structure. *Biochemistry.* 40:3828–3846.

Cortes, D., L. Cuello, and E. Perozo. 2001. Molecular architecture of full-length KcsA: role of cytoplasmic domains in ion permeation and activation gating. *J. Gen. Physiol.* 117:165–180.

Cruickshank, C.C., R.F. Minchin, A.C. Le Dain, and B. Martinac. 1997. Estimation of the pore size of the large-conductance mechanosensitive ion channel of Escherichia coli. *Biophys. J.* 73:1925–1931.

Cuello, L.G., J.G. Romero, D.M. Cortes, and E. Perozo. 1998. pH-dependent gating in the *Streptomyces lividans* K^+ channel. *Biochemistry.* 37:3229–3236.

Elmore, D.E., K.D. Phillipson, and D.A. Dougherty. 2001. Molecular dynamics symulations of the *M. tuberculosis* mechanosensitive channel of large conductance. *Biophys. J.* 80:110a. (Abstr.)

Farahbakhsh, Z.T., C. Altenbach, and W.L. Hubbell. 1992. Spin labeled cysteines as sensors for protein-lipid interaction and conformation in rhodopsin. *Photochem. Photobiol.* 56:1019–1033.

Fraczkiewicz, R., and W. Braun. 1998. Exact and efficient analytical calculation of the accessible surface areas and their gradients for macromolecules. *J. Comp. Chem.* 19:319–333.

Hamill, O.P., and D.W. McBride. 1997. Induced membrane hypo/hyper-mechanosensitivity: a limitation of patch-clamp recording. *Annu. Rev. Physiol.* 59:621–631.

Hamill, O.P., and B. Martinac. 2001. Molecular basis of mechano-transduction in living cells. *Physiol. Rev.* 81:685–740.

Häse, C.C., A.C. Le Dain, and B. Martinac. 1995. Purification and functional reconstitution of the recombinant large mechanosensitive ion channel (MscL) of *Escherichia coli. J. Biol. Chem.* 270:18329–18334.

Hubbell, W.L., D.S. Cafiso, and C. Altenbach. 2000. Identifying conformational changes with site-directed spin labeling. *Nat. Struct. Biol.* 7:735–739.

Kabsch, W., and C. Sander. 1983. Dictionary of protein secondary structure: pattern recognition of hydrogen-bonded and geometrical features. *Biopolymers.* 22:2577–2637.

Kleywegt, G.J., and T.A. Jones. 1994. Detection, delineation, measurement and display of cavities in macromolecular structures. *Acta Crystallographica D.* 50:178–185.

Kloda, A., and B. Martinac. 2001. Molecular identification of a mechanosensitive channel in archaea. *Biophys. J.* 80:229–240.

Levina, N., S. Totemeyer, N.R. Stokes, P. Louis, M.A. Jones, and I.R. Booth. 1999. Protection of *Escherichia coli* cells against extreme turgor by activation of MscS and MscL mechanosensitive channels: identification of genes required for MscS activity. *EMBO J.* 18:1730–1737.

Martinac, B. 2001. Mechanosensitive Channels in Prokaryotes. *Cell. Physiol. Biochem.* 11:61–76.

Martinac, B., M. Buechner, A.H. Delcour, J. Adler, and C. Kung. 1987. Pressure-sensitive ion channel in *Escherichia coli. Proc. Natl. Acad. Sci. USA.* 84:2297–2301.

Martinac, B., J. Adler, and C. Kung. 1990. Mechanosensitive ion channels of *E. coli* activated by amphipaths. *Nature.* 348:261–263.

Martinac, B., A. Kloda, and E. Perozo. 2000. Structural dynamics of *MscL* first transmembrane segment. a site directed spin-labeling study. *Biophys. J.* 78:137a. (Abstr.)

Mchaourab, H., and E. Perozo. 2000. Determination of protein folds and conformational dynamics using spin-labeling EPR Spectroscopy. *In* Biological Magnetic Resonance. Vol. 19. G.E.S. Eaton, and L. Berliner, editors. Kluwer-Plenum, New York. 155–218.

Mchaourab, H.S., M.A. Lietzow, K. Hideg, and W.L. Hubbell. 1996. Motion of spin-labeled side chains in T4 lysozyme. Correlation with protein structure and dynamics. *Biochemistry.* 35:7692–7704.

Moe, P.C., P. Blount, and C. Kung. 1998. Functional and structural conservation in the mechanosensitive channel MscL implicates elements crucial for mechanosensation. *Mol. Microbiol.* 28:583–592.

Nicholls, A., K.A. Sharp, and B. Honig. 1991. Protein folding and association: insights from the interfacial and thermodynamic properties of hydrocarbons. *Proteins.* 11:281–296.

Oakley, A.J., B. Martinac, and M.C. Wilce. 1999. Structure and function of the bacterial mechanosensitive channel of large conductance. *Prot. Sci.* 8:1915–1921.

Perozo, E., D.M. Cortes, and L.G. Cuello. 1998. Three-dimensional architecture and gating mechanism of a K$^+$ channel studied by EPR spectroscopy. *Nat. Struct. Biol.* 5:459–469.

Perozo, E., D.M. Cortes, A. Kloda, and B. Martinac. 2001. Structural dynamics of *MscL* outer transmembrane segment. A site directed spin-labeling study. *Biophys. J.* 80:345a. (Abstr.)

Rees, D.C., G. Chang, and R.H. Spencer. 2000. Crystallographic analyses of ion channels: lessons and challenges. *J. Biol. Chem.* 275:713–716.

Spencer, R.H., G. Chang, and D.C. Rees. 1999. 'Feeling the pressure': structural insights into a gated mechanosensitive channel. *Curr. Opin. Struct. Biol.* 9:448–454.

Subczynski, W.K., and J.S. Hyde. 1981. The diffusion-concentration product of oxygen in lipid bilayers using the spin-label T1 method. *Biochim. Biophys. Acta.* 643:283–291.

Sukharev, S.I., B. Martinac, V.Y. Arshavsky, and C. Kung. 1993. Two types of mechanosensitive channels in the *Escherichia coli* cell envelope: solubilization and functional reconstitution. *Biophys. J.* 65:177–183.

Sukharev, S.I., P. Blount, B. Martinac, F.R. Blattner, and C. Kung. 1994. A large-conductance mechanosensitive channel in E. coli encoded by mscL alone. *Nature.* 368:265–268.

Sukharev, S.I., P. Blount, B. Martinac, and C. Kung. 1997. Mechanosensitive channels of *Escherichia coli*: the MscL gene, protein, and activities. *Annu. Rev. Physiol.* 59:633–657.

Sukharev, S.I., W.J. Sigurdson, C. Kung, and F. Sachs. 1999. Energetic and spatial parameters for gating of the bacterial large conductance mechanosensitive channel, MscL. *J. Gen. Physiol.* 113: 525–540.

Sukharev, S.I., M. Betanzos, C.-S. Chiang, and H.R. Guy. 2001. The gating mechanism of the large mechanosensitive channel MscL. *Nature.* 409:720–724.

Thompson, J., D.G. Higgins, and T.J. Gibson. 1994. CLUSTAL W: improving the sensitivity of progressive multiple sequence alignment through sequence weighting, position specific gap penalties and weight matrix choice. *Nucleic Acids Res.* 22:4673–4680.

Yoshimura, K., A. Batiza, and C. Kung. 2001. Chemically charging the pore constriction opens the mechanosensitive channel MscL. *Biophys. J.* 80:2198–2206.

Yoshimura, K., A. Batiza, M. Schroeder, P. Blount, and C. Kung. 1999. Hydrophilicity of a single residue within MscL correlates with increased channel mechanosensitivity. *Biophys. J.* 77:1960–1972.